EARTH SCIENCES
RESEARCH JOURNAL
Earth Sci. Res. J. Vol. 29, No. 1 (March, 2025): 69 - 80

UNIVERSIDAD NACIONAL DE COLOMBIA

GEOTECHNICS

Freeze–thaw–induced microstructural alterations and deterioration of physico-mechanical properties in rocks from the himalayan ranges (Pakistan)

Abid Nawaz[1]*, Muhammad Sajid[2,3], Waqas Ahmed[1], Abdul Rahim Asif[1]
1. National Centre of Excellence in Geology, University of Peshawar, Peshawar 25120, Pakistan
2. Department of Geology, University of Peshawar, Peshawar, 25120, Pakistan
3. Helmholtz-Zentrum Potsdam, Deutsches GeoForschungsZentrum (GFZ), Telegrafenberg, Potsdam, Germany
*Corresponding Author: Abid Nawaz, Email: abidgeo88@uop.edu.pk

ABSTRACT

This study investigates in detail the impact of freeze-thaw cycles on the physical and mechanical properties of a variety of rock types, including granulite, amphibolite, limestone, sandstone, granitic gneiss, quartzite, rhyolite, dolerite, and gabbronorite. The selected rock samples underwent several freeze-thaw cycles at temperatures ranging from 25°C to -40°C. After these cycles, tests were performed to assess the response of the rocks to varying temperatures. Destructive tests (uniaxial compressive strength, point load index) and non-destructive testing (specific gravity, ultrasonic pulse wave velocity, porosity, and water absorption) were carried out. The density of the induced fractures in each type of rock under investigation was calculated. The fracture density in the samples increased as the number of cycles increased. After fifty cycles, the fracture density of selected rocks increased as follows: 1.12% for sandstone, 1.06% for limestone, 0.59% for rhyolite, 0.48% for gabbronorite, 0.57% for quartzite, 0.76% for granitic gneiss, 0.46% for amphibolite, and 0.43% for granulite. The extent and strength of the fractures increased further with continued cycles. After 100 freeze-thaw cycles, the fracture densities rose to 1.47%, 1.44%, 1.22%, 1.05%, 1.14%, 1.31%, 1.03%, and 1.02%, respectively. Similarly, porosity and water absorption levels showed an increased trend. However, as the freeze-thaw process continues, the results indicate a decrease in uniaxial compressive strength (UCS), specific gravity, ultrasonic pulse velocity (UPV), and point load strength. These findings highlight how freeze-thaw conditions deteriorate rocks and change their physico-mechanical characteristics, with significant implications for the mining and building sectors.

Keywords: Diverse rock suites, Freeze-thaw cycles, Physico-mechanical properties, Fracture density, Mechanical strength

Alteraciones microestructurales y deterioro de las propiedades físico-mecánicas por ciclos de congelación-deshielo inducidos en rocas del Himalaya paquistaní

RESUMEN

Este estudio investiga en detalle el impacto de los ciclos de congelación-deshielo en las propiedades físicas y mecánicas de una variedad de tipos de rocas en las que se incluyen granulitas, anfibolitas, calizas, areniscas, gneises graníticos, cuarcitas, riolitas, doleritas y gabronoritas. Las muestras de roca fueron sometidas a varios ciclos de congelación-deshielo a temperaturas que oscilaron entre 25 °C y -40 °C. Después de estos ciclos se realizaron las evaluaciones para medir la respuesta de las rocas a la variación de las temperaturas. Se realizaron evaluaciones destructivas (resistencia a la compresión uniaxial, índice del punto de carga) y no destructivas (gravedad específica, velocidad de onda de pulso ultrasónico, porosidad y absorción de agua). Luego se calculó la densidad de las fracturas ocasionadas en cada tipo de muestras de roca. La densidad de la fractura en las muestras se incrementó a medida que se incrementó el número de ciclos. Después de 50 ciclos la densidad de la fractura de las rocas seleccionadas se incrementa de la siguiente manera: 1.12 % para las areniscas, 1.06 % para las calizas, 0.5 % para las riolitas, 0.48 % para las gabronoritas, 0.57 % para las cuarcitas, 0.76 % para los gneises graníticos, 0.46 % para las anfibolitas y 0.43 % para las granulitas. El alcance y fortaleza de las fracturas se incrementa a medida que los ciclos continuan. Después de 100 ciclos, la densidad de las fracturas alcanza el 1.47 %, 1.44 %, 1.22 %, 1.05 %, 1.14%, 1.31%, 1.03%, y 1.02%, en el mismo orden del enunciado anterior. De igual manera, los niveles de porosidad y absorción de agua muestran una tendencia de crecimiento. Sin embargo, mientras que los ciclos de congelación-deshielo continuan, los resultados señalan un decrecimiento en la resistencia a la compresión uniaxial, la gravedad específica, la velocidad de onda de pulso ultrasónico y en el índice de punto de carga. Estos hallazgos resaltan como las condiciones de los ciclos de congelación-deshielo deterioran las rocas y cambian sus características físico-químicas, con las implicaciones que esto trae para los sectores de la minería y la construcción.

Palabras clave: muestra de rocas; ciclos de congelación-deshielo; propiedades físico-químicas; densidad de la fractura; fortaleza mecánica

Record
Manuscript received: 09/09/2024
Accepted for publication: 10/03/2025

How to cite item:
Nawaz, A., Sajid, M., Ahmed, W., & Asif, A. R. (2025). Freeze–thaw–induced microstructural alterations and deterioration of physicomechanical properties in rocks from the Himalayan ranges (Pakistan). *Earth Sciences Research Journal, 29*(1), 69-80. https://doi.org/10.15446/esrj.v29n1.116550

ISSN 1794-6190 e-ISSN 2339-3459
https://doi.org/10.15446/esrj.v29n1.116550

1 Introduction

Freeze-thaw cycles significantly affect the strength and durability of rocks, especially in cold regions or areas where temperatures occasionally dip below freezing. This environmental stress causes rocks to degrade due to factors such as moisture content, rock type, and the frequency of freeze-thaw cycles (Zhao et al., 2024). These effects pose challenges to various industries, including construction, railroads, and the preservation of stone monuments (Talalay, 2022; 2023). As such, understanding rock resistance to freeze-thaw-induced deterioration is crucial when selecting building materials (Asif et al., 2022; 2024).

Although freeze-thaw damage is more prominent in colder climates, it also occurs in regions with intermittent freezing temperatures, particularly during nightly freezes (Kaczmarek et al., 2021). The repeated freezing and thawing of water within the rock's pores generates internal pressure, which leads to microfractures and reduced strength (Chen et al., 2023). These processes significantly influence various physical and mechanical properties, including porosity, permeability, and compressive strength (Liu et al., 2020; Mal'a et al., 2024).

The resistance of rocks to freeze-thaw cycles is strongly influenced by their mineral composition, texture, and structural properties. Sedimentary rocks such as limestone and sandstone, composed of calcite, dolomite, quartz, and feldspar, are generally more vulnerable due to their higher porosity and the susceptibility of calcite to dissolution (Deprez et al., 2020). Sandstone deteriorates due to intergranular fractures that allow water infiltration during freeze thaw process (Niu et al., 2021). Furthermore, metamorphic rocks, including amphibolite, granulite, and quartzite, exhibit greater resistance due to their recrystallized and interlocking mineral structures (Citak et al., 2023). Amphibolite and granulite, consisting of amphibole, garnet, pyroxene, and quartz, have low porosity, limiting water ingress, though pre-existing fractures may serve as weakness zones (Islands et al., 2002). Quartzite, being primarily composed of quartz, is highly resistant but can develop microcracks over time (Hou et al., 2025). Moreover, igneous rocks display varied behavior during freeze thaw process. Rhyolite, with its fine-grained texture and high silica content, is prone to microcracking (Schwamborn et al., 2012). Moreover, dolerite and gabbronorite, composed of pyroxene, olivine, and plagioclase, exhibit higher durability due to their crystalline structure and lower porosity (Claridge and Campbell, 2005).

This study aims to investigate the effects of freeze-thaw cycles on the mechanical and physical properties of nine rock types, selected based on their varied characteristics (Table 1). The rocks were divided into three groups: untreated, exposed to 50 cycles, and exposed to 100 cycles. The experimental approach involved assessing properties such as porosity, specific gravity, pulse velocity (Vp), unconfined compressive strength (UCS), point load strength, and water absorption. Additionally, fracture density was quantified and statistically compared with the engineering properties after specific freeze-thaw cycles through regression analysis.

While previous studies have explored freeze-thaw effects on various rocks, this research bridges a gap by focusing on a diverse set of rock types under controlled laboratory conditions, allowing for a deeper understanding of how different rocks respond to repeated freeze-thaw stresses. The novelty of this study lies in its comprehensive approach to comparing the impacts of freeze-thaw cycles on multiple rock types and correlating these effects with changes in mechanical performance, providing valuable insights for industries that rely on rock durability in cold environments.

2 Geology of northern Pakistan

In northwest Pakistan, there are three primary tectonic domains: the Indian plate, the Kohistan Island Arc (KIA), and the Eurasian plate. The KIA originated from intra-oceanic subduction in the Tethys Ocean and collided with the Indian plate at the Main Mantle Thrust (MMT) regional fault zone (Fig. 1) (Searle and Treloar, 2010; Burg, 2018). To the north of Kohistan Island Arc, the primary sutures of the Main Karakoram Thrust (MKT) mark its boundary with the Karakoram block. Two collisional events, first with the Eurasian plate and later with the Indian plate, resulted in complicated deformation and metamorphism of the KIA rocks (Suo et al., 2022). The KIA is made up of sedimentary, volcanic, and plutonic rocks and is divided into six main sections (Ali et al., 2021). The mafic and ultramafic Jijal complex is the deepest area of the KIA and it marks the transition between the upper mantle and lower crust (Ali et al., 2021; Ullaha et al., 2022). The Kamila Amphibolite belt was formed by the metamorphism of the gabbroic and mafic to intermediate metavolcanics up to the amphibolite facies (Rehman and Arif, 2020). The Chilas Complex is a large-scale late Cretaceous magmatic structure located north of Kamila amphibolite. It is largely made of gabbronorite, with smaller amounts of troctolite, quartz-diorite, and gabbro (Lutfi et al., 2023). The Kohistan batholith is made up of Early Cretaceous Chalt Volcanics with andesitic lavas, tuffs, agglomerates, and calc-alkaline granitoids (Jadoon et al., 2020; Ali et al., 2021). Greywackes, pelites, and volcano-clastic rocks form the rocks of the Yasin and Chalt groups in the northern KIA (Qureshi et al., 2020).

The three tectonic units that comprise the northern Indian plate to the south are the Lesser Himalayan Sequence (LHS), the Greater Himalayan Sequence (GHS), and the Tethyan Himalayan Sequence (THS). The Main Central Thrust (MCT) and the South Tibetan Detachment System (STDS) are the two regional fault systems that split these units (Fig. 1). Different granitic suites have been detected in the Himalayan terrane: early Paleozoic suites brought about by accretionary orogenesis, late Paleozoic suites connected to the rift, and early Cenozoic suites connected to the Himalayan collision (Sajid et al., 2018; Jain et al., 2020; Soret et al., 2021; Sen et al., 2022).

Northern Pakistan experiences a diverse climate, ranging from temperate to alpine conditions due to its high-altitude terrain. The region undergoes significant seasonal temperature variations, with summer temperatures exceeding 30°C in lower valleys, while winter temperatures in higher elevations frequently drop below freezing. These fluctuations lead to repeated freeze-thaw cycles, particularly in areas above 2,500 meters where diurnal temperature variations cross the freezing threshold. Additionally, substantial precipitation, including monsoonal rains and heavy snowfall, contributes to rock saturation, enhancing the susceptibility of various lithologies to freeze-thaw weathering. This climatic setting makes freeze-thaw processes a dominant factor in rock degradation, slope instability, and infrastructure deterioration in the region.

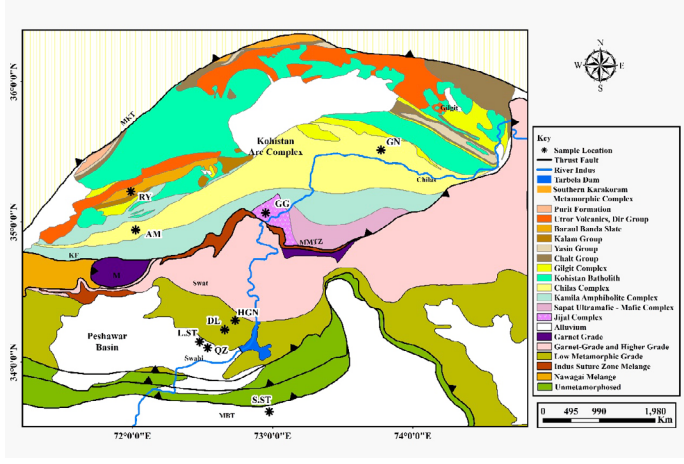

Figure 1. Geological map of the Western Himalayas in Pakistan. Modified after DiPietro et al., 2001. The black stars show the studied sample location. RY=Rhyolite; AM=Amphibolite; DL=Dolerite; L.ST=Limestone; QZ=Quartzite; HGN= Hazara Granitic Gneiss; S.ST=Sandstone; GN=Gabbronorite; GG=Granulite.

3 Methods

3.1 Preparation of Samples and Freeze-Thaw Cycling

The mineralogical composition, geographic positions, and grain size descriptions of the rocks under investigation are given in Table 1. During

fieldwork, bulk samples of these rock types were collected, from which cubic inch-sized samples were extracted. These samples were then analyzed at the National Centre of Excellence in Geology (NCEG), University of Peshawar. These cubic specimens underwent a series of freeze-thaw cycles, each lasting eight hours. During each cycle, the samples were exposed to -40°C for 4 hours followed by thawing at room temperature (25°C) for the remaining 4 hours. The investigations included subjecting the samples to 50 and 100 cycles. Following the freeze-thaw cycles, thin sections were prepared from the samples to analyze changes in their respective petrographic properties. Fig. 2 shows the steps involved in conducting this research work.

3.2 Fracture delineation

For a more thorough analysis of the samples' internal structure and related variations, thin sections were prepared from the samples. These thin sections were photomicrographed using petrographic microscopes. Individual fractures seen in the photomicrographs of the treated samples were highlighted and compared with the thin section observation of untreated samples (room temperature) using the ImageJ program. The area and extent of each fracture present in the photomicrographs were precisely calculated, and the total area of the rock specimen mounted on the thin section was determined. Fracture density was assessed using the following formula:

Fracture density = 100% - (Area of thin section-Area of Fractures)/Area of thin section * 100

While examining thin sections to find cracks caused by freeze-thaw (F-T) cycling, specific features were considered. At first, different fracture patterns were seen in the treated and untreated samples. These patterns included straight or curved lines crossing or passing through the rock matrix. These cracks may appear in the thin section as black isotropic streaks or discontinuities. Leaching near the fractures, which caused observable color changes or staining patterns after therapy, was another important sign. In the thin section, F-T-generated cracks showed broad discontinuities cutting through several mineral grains, a characteristic absent from untreated materials. These fractures are distinguished from other kinds of discontinuities or cleavages because of their irregular and jagged patterns. The gabbronorite sample treated with 50 F-T CYCLES is shown in Fig. 3, where fractures are indicated by green lines. In Fig. 3, fractures are shown in relation to the overall area taken into consideration in the thin section.

Table 1. Descriptions of the rocks under investigation

S. No	Rock type	Symbol	Geological Unit	Coordinates	Mineralogy	Grain Size
1	Dolerite	DL	Panjal Dykes	34.23113000 72.65824833	Clinopyroxene Plagioclase Olivine	Medium grained
2	Rhyolite	RY	Dir Volcanics	35.21587866 71.98874537	Orthopyroxene Clinopyroxene Plagioclase	Fine grained
3	Gabbronorite	GN	KIA	35.511531 73.773089	Calcium-rich plagioclase Hypersthene Orthopyroxene	Coarse grained
4	Sand stone	S.ST	Murree Formation	33.64813945 72.97608807	Quartz Potash Feldspar Biotite	Coarse grained
5	Limestone	L.ST	Nowshera Formation	34.14549205 72.47979880	Calcite Dolomite	Fine grained
6	Quartzite	QZ	Tanawal Formation	34.10182333 72.53580833	Quartz Biotite	Medium to Coarse grained
7	Granitic gneiss	HGN	Hazara Granitic Gneiss	34.29825500 72.73238000	Quartz, Potassium feldspar Sodium feldspar	Coarse grained
8	Amphibolite	AM	KIA	34.94245500 72.02215000	Hornblende Plagioclase Quartz	Coarse grained
9	Granulite	GG	KIA	35.063864 72.949761	Amphibole Clinopyroxene Garnet Quartz	Medium to Coarse grained

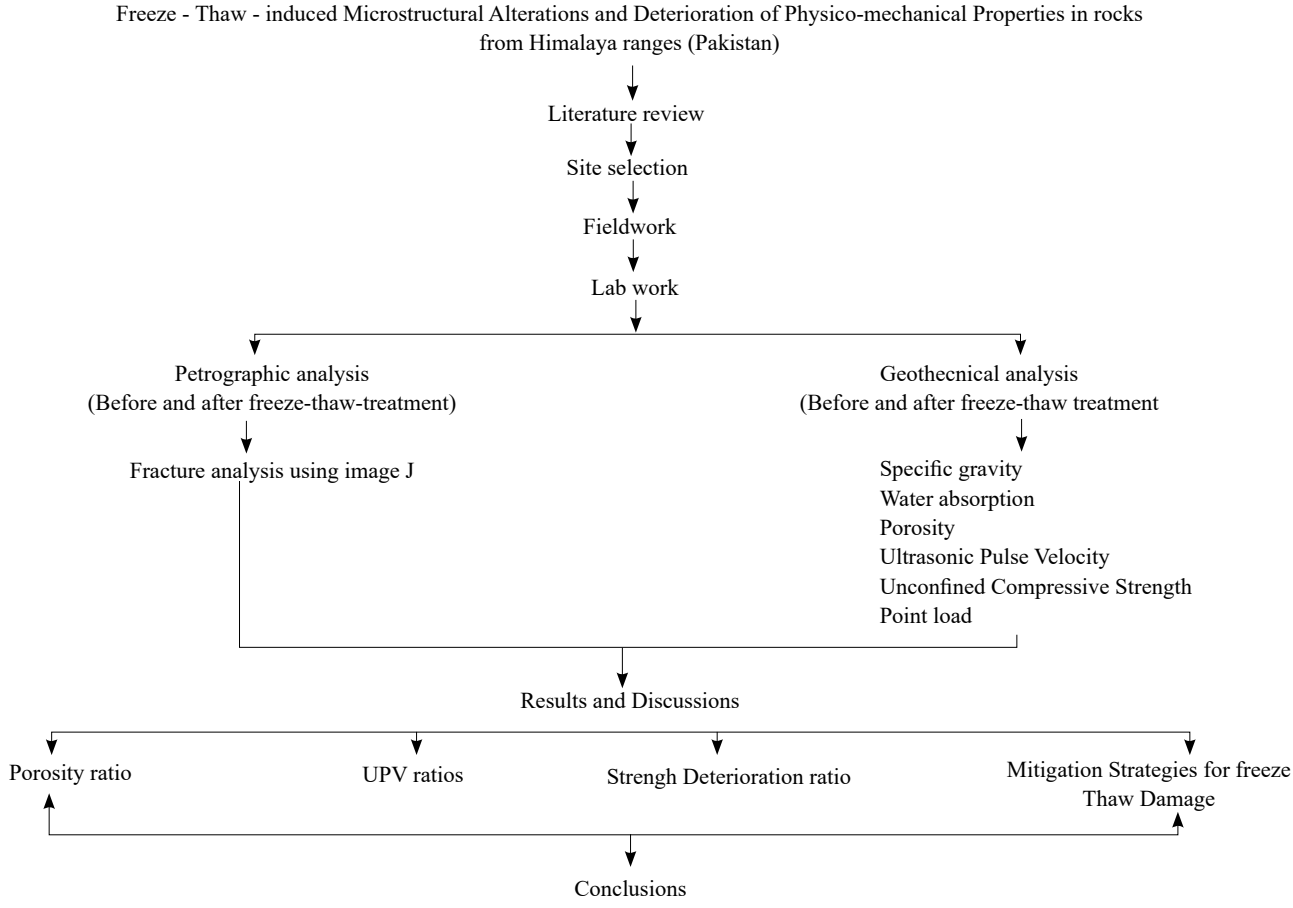

Figure 2. Flowchart illustrates the approaches employed in this research study

3.3 Physical and mechanical testing

The treated samples' mechanical properties (unconfined compressive strength and point load test) and physical properties (specific gravity, water absorption, porosity, and ultrasonic pulse velocity) were evaluated in accordance with the standards set by the American Society for Testing and Materials (ASTM).

A pitch-catch method, using a transmitter and a receiver as two transducers, was used to calculate the ultrasonic pulse velocity (UPV) for each specimen (ASTM-D-2845-08). The samples were weighed in the following conditions: air, water, oven-dry, and saturated in water for an entire day. Following this, the bulk water absorption, bulk saturated specific gravity (DC97/C97M-18), and bulk porosity were determined using the formulas outlined below:

Water absorption = (Water saturated weight – Dry weight)/Dry weight

Specific gravity = Saturated weight/ (Saturated weight – Weight in water)

Porosity = (Weight in air – Dry weight)/ (weight in air – weight in water)

The unconfined compressive strength and Point load testing were carried out as per ASTM (D7012–14e1) and ASTM (D 5731) respectively

4. Petrography

The petrographic analysis of the rock samples revealed distinct mineralogical, textural, and structural characteristics for each rock type, as summarized below:

4.1 Rhyolite (RY):

Rhyolite from the Dir Volcanics is fine-grained with a porphyritic texture. The groundmass consists of microcrystalline quartz and feldspar, with phenocrysts of orthopyroxene, clinopyroxene, and plagioclase (Fig. 4 A). The feldspar phenocrysts exhibit perthitic textures, and quartz grains show undulatory extinction.

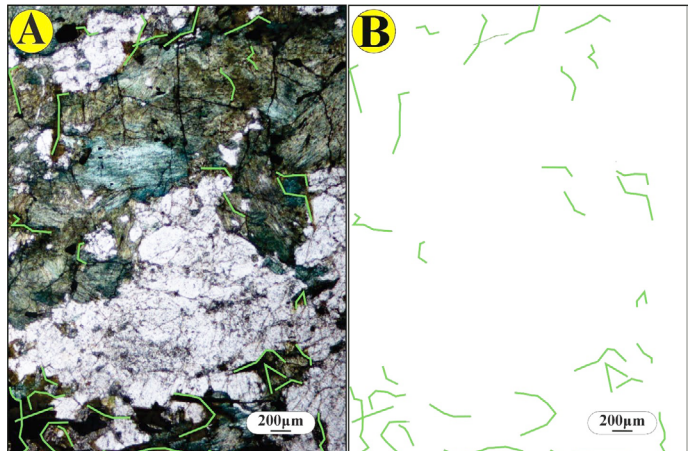

Figure 3. Fracture pointed out after 50 freeze-thaw cycles in gabbronorite

4*4.2 Dolerite (DL):*

Dolerite samples, collected from the Panjal Dykes, exhibit a medium-grained texture dominated by clinopyroxene, plagioclase, and olivine (Fig. 4 B). The clinopyroxene grains display high relief and weak pleochroism, while plagioclase appears as tabular grains with polysynthetic twinning. Olivine is present as subhedral to anhedral grains, often showing signs of alteration.

4.3 Gabbronorite (GN):

Gabbronorite samples from the Kohistan Island Arc (KIA) are coarse-grained, with calcium-rich plagioclase, hypersthene, and orthopyroxene as the primary minerals (Fig. 4 C). Plagioclase grains display polysynthetic twinning, while orthopyroxene exhibits weak pleochroism. The interlocking texture of the minerals contributes to the rock's durability.

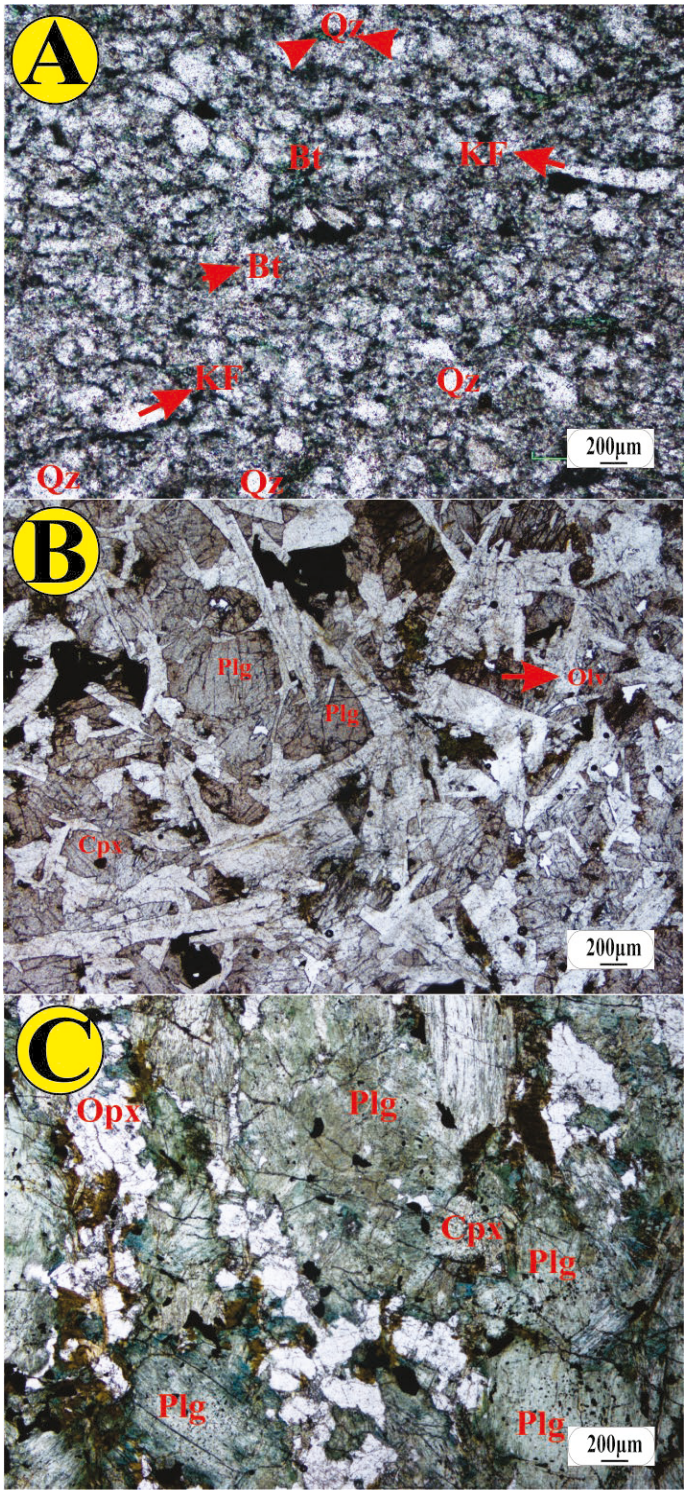

Figure 4. Photomicrographs of thin sections of igneous rocks under polarized light. (A) Rhyolite composed of quartz (Qz), biotite (Bt), and potash feldspar (KF); (B) Dolerite consisting of clinopyroxene (Cpx), olivine (Olv), and plagioclase (Plg); (C) Gabbronorite composed of plagioclase (Plg), orthopyroxene (Opx), and clinopyroxene (Cpx).

4.4 Limestone (L.ST):

Limestone samples from the Nowshera Formation are fine-grained, predominantly composed of calcite and dolomite (Fig. 5 A). Calcite grains exhibit characteristic birefringence, while dolomite appears as subhedral to anhedral grains, sometimes showing twinning. The rock has a crystalline texture with occasional microfossil fragments.

4.5 Sandstone (S.ST):

Sandstone from the Murree Formation is coarse-grained, composed primarily of quartz, potash feldspar, and biotite (Fig. 5B). Quartz grains are rounded to subangular, showing undulatory extinction, while biotite occurs as elongated, pleochroic flakes. The intergranular spaces are often filled with secondary cementing materials.

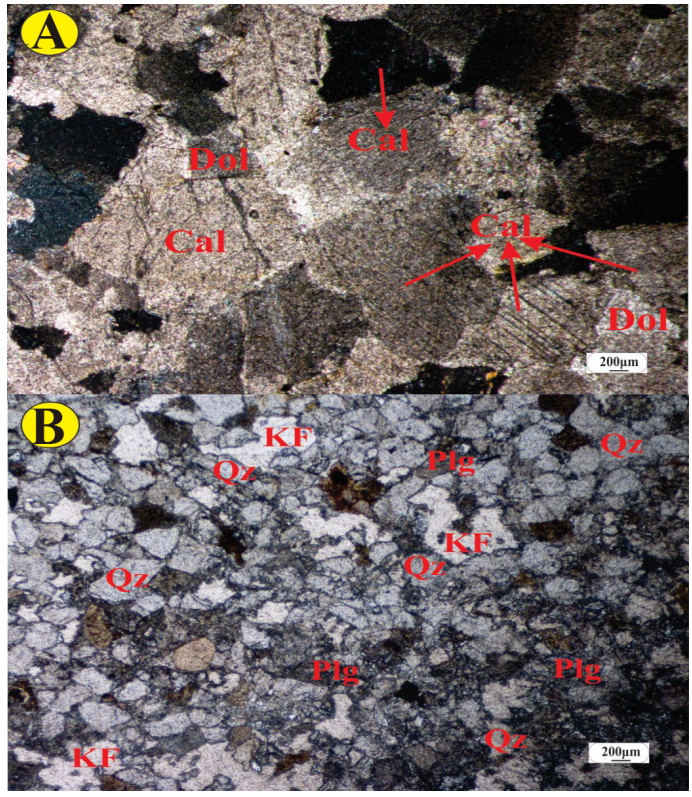

Figure 5. Photomicrographs of thin sections of sedimentary rocks under polarized light. (A) Limestone primarily composed of calcite (Cal) and dolomite (Dol); (B) Sandstone consisting of quartz (Qz), biotite (Bt), and potash feldspar (KF).

4.6 Amphibolite (AM):

Amphibolite samples from the KIA are coarse-grained, composed of hornblende, plagioclase, and quartz (Fig. 6 A). Hornblende exhibits strong pleochroism from green to brown, while plagioclase displays polysynthetic twinning. The rock has a foliated texture due to the alignment of hornblende crystals.

4.7 Granulite (GG):

Granulite from the KIA is medium to coarse-grained, with amphibole, clinopyroxene, garnet, and quartz as the primary minerals (Fig. 6B). Garnet appears as isotropic, subhedral to euhedral grains, while clinopyroxene shows high relief. The rock has a granoblastic texture with interlocking mineral grains.

4.8 Granitic Gneiss (HGN):

Hazara Granitic Gneiss is coarse-grained, with quartz, potassium feldspar, and sodium feldspar as the primary minerals (Fig. 6 C). The rock exhibits a gneissic texture with distinct mineral banding. Quartz grains show undulatory extinction, while feldspars display perthitic textures.

4.9 Quartzite (QZ):

Quartzite from the Tanawal Formation is medium to coarse-grained, with quartz as the dominant mineral and minor biotite (Fig. 6 D). The quartz grains show interlocking textures with sutured contacts, indicative of metamorphic recrystallization. Biotite occurs as scattered flakes within the quartz matrix.

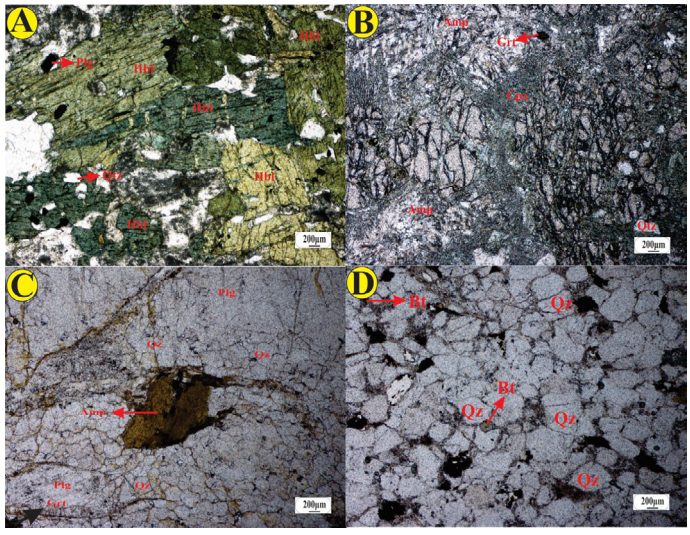

Figure 6. Photomicrographs of thin sections of metamorphic rocks under polarized light. (A) Amphibolite composed of plagioclase (Plg), hornblende (Hbl), and quartz (Qz); (B) Granulite consisting of amphibole (Amp), garnet (Grt), clinopyroxene (Cpx), and quartz (Qz); (C) Hazara Granitic Gneiss comprising amphibole (Amp), quartz (Qz), garnet (Grt), and plagioclase (Plg); (D) Quartzite composed primarily of quartz (Qz) and biotite (Bt).

5 Results

5.1 Impacts of Mineralogical composition on Freeze-Thaw Cycling

The mineralogical composition of the rock types significantly influences their resistance to freeze-thaw cycles by affecting their porosity, permeability, and mechanical strength. Sedimentary rocks, such as limestone and sandstone, contain minerals like calcite, dolomite, quartz, and feldspar, which exhibit varying responses to freeze-thaw weathering. Limestone, being rich in calcite and dolomite, is more susceptible to freeze-thaw damage due to dissolution and microcrack propagation along grain boundaries. Sandstone, primarily composed of quartz and feldspar, exhibits moderate resistance, though intergranular fractures can facilitate water infiltration and enhance degradation over repeated freeze-thaw cycles.

Metamorphic rocks generally exhibit higher resistance to freeze-thaw cycles due to their recrystallized textures and interlocking mineral structures. Amphibolite and granulite, composed of amphibole, garnet, pyroxene, and quartz, have relatively low porosity, reducing their susceptibility to water infiltration. However, pre-existing fractures and foliation planes can act as weak zones where freeze-thaw action may induce further damage. Quartzite, predominantly composed of quartz, demonstrates high resistance due to its compact texture, though microcracks within quartz grains may contribute to localized weakening.

Igneous rocks display variable resistance depending on their mineral composition and cooling history. Rhyolite, with its high silica content and fine-grained texture, is prone to microcracking and freeze-thaw deterioration, particularly along feldspar and quartz phenocrysts. Dolerite and gabbronorite, composed of pyroxene, olivine, and plagioclase, generally exhibit higher resistance due to their crystalline structure and lower porosity. However, intergranular fractures and thermal contraction cracks may serve as pathways for water infiltration, potentially accelerating degradation under repeated freeze-thaw cycling.

5.2 Freeze-thaw-induced fractures

The fracture density in the samples under investigation increased with the number of cycles (Fig. 7). Following fifty cycles, the fracture density for different types of rocks increased as follows: 1.12% for sandstone, 1.06% for limestone, 0.59% for rhyolite, 0.48% for gabbronorite, 0.57% for quartzite, 0.76% for granitic gneiss, 0.46% for amphibolite, and 0.43% for granulite (Fig. 7). The extent and strength of the fractures increase as the cycles continue. Its fracture densities are increased to 1.47%, 1.44%, 1.22%, 1.05%, 1.14%, 1.31%, 1.03%, and 1.02%, respectively, following 100 freeze-thaw cycles. Granulite exhibits the greatest resistance to freeze-thaw, however, sandstone and limestone are very susceptible to fragmentation after cycles of freezing and thawing (Fig. 8).

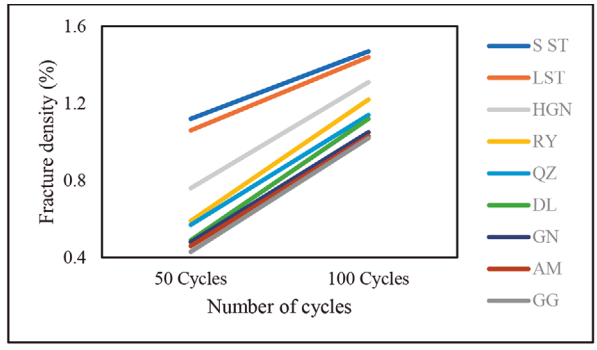

Fig. 7. The fracture density of rock samples following different freeze-thaw cycles

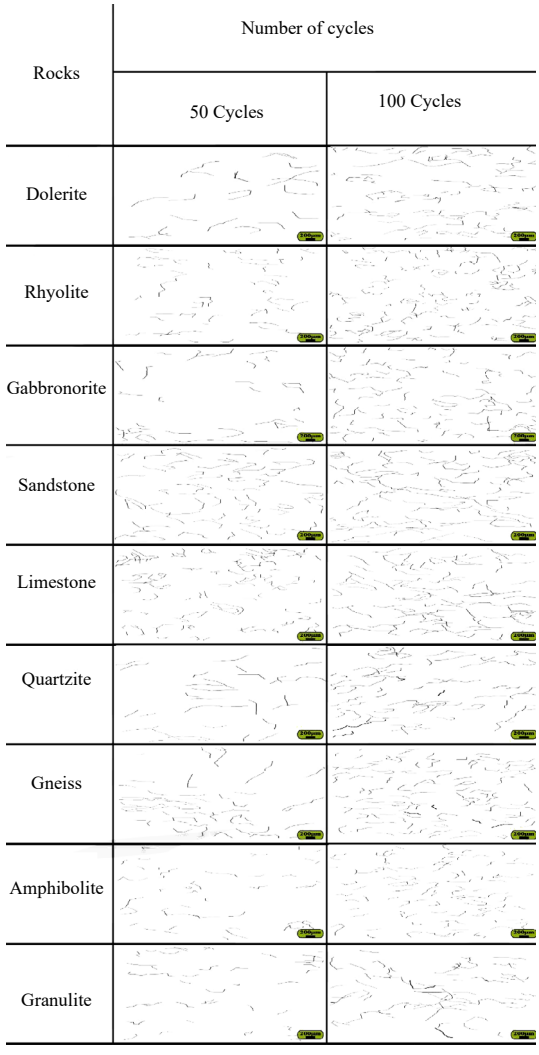

Figure 8. The distribution of fractures in rocks with an increasing number of freeze-thaw cycles

5.3 UCS

Fig. 9A shows the unconfined compressive strength (UCS) values following treatment cycles and at room temperature. Test results show that limestone loses strength very gradually, but sandstone loses strength more quickly than limestone. Granulite had the highest strength following cycles and the strongest resilience among all the samples under study (Fig. 9A). Its total percentage strength drop during freeze-thaw cycling is also less than that of other forms of rock. After 50 cycles, the UCS decreased by the following percentages: granitic gneiss by 8.82%, rhyolite by 7.41%, quartzite by 5.43%, dolerite by 4.55%, gabbronorite by 3.31%, amphibolite by 2.33%, and granulite by 1.49%. As previously indicated, sandstone and limestone were severely impacted; after 50 freeze-thaw cycles, the UCS of limestone decreased by 10.20% and that of sandstone by 14.29%. A further decrease in UCS occurred as the number of cycles rose. Following 100 cycles, the UCS decreased by the following percentages: granitic gneiss by 17.65%, rhyolite by 13.58%, dolerite by 10%, quartzite by 11.95%, gabbronorite by 7.43%, amphibolite by 6.98%, and granulite by 4.47%. After 100 freeze-thaw cycles, the UCS of limestone decreased by 22.45% and that of sandstone by 28.57%.

5.4 Point load

The results clearly show that the point load strength of the studied rock samples is significantly impacted by freeze-thaw cycling. The change in point load strength is minimum when rocks are subjected to freeze-thaw cycles. However, as the number of F-T cycles increases, there is a significant and notable decrease in point load strength (Fig. 9B). After 100 freeze-thaw cycles, the point load of the rocks decreases by the following percentages: granitic gneiss by 20.58%, rhyolite by 17.95%, quartzite by 13.95%, dolerite by 10.20%, gabbronorite by 9.8%, amphibolite by 7.14%, and granulite by 6.25%. Additionally, sandstone experiences a 33.33% reduction, while limestone undergoes a 25% reduction after 100 cycles.

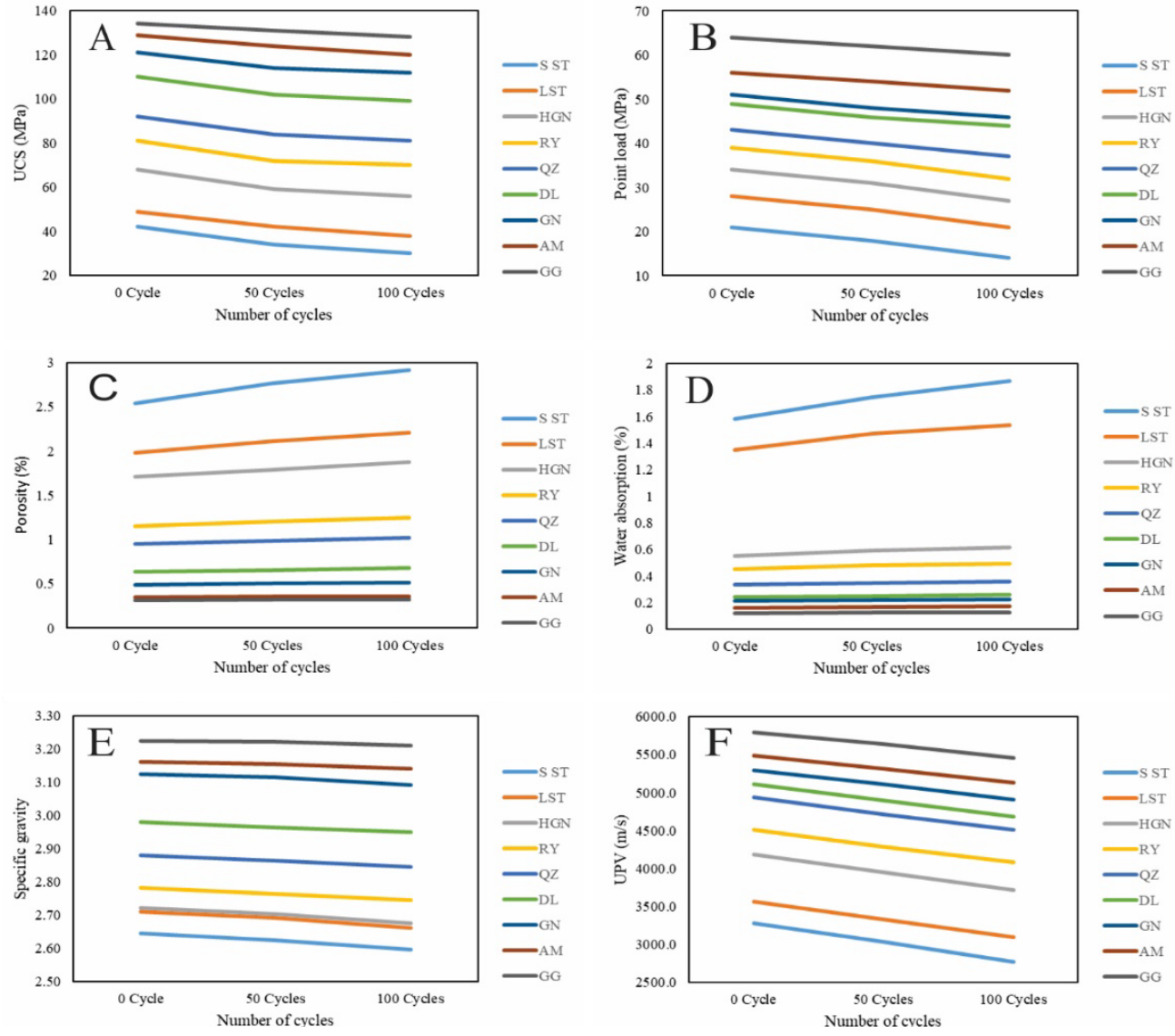

Figure 9. The impact of freeze-thaw on different physico-mechanical properties of rocks. Figure 9A illustrates Unconfined compressive strength (UCS), B showcases Point load strength, C presents Porosity, D displays Water absorption, E represents Specific gravity and F shows Ultrasonic pulse velocity (UPV)

Table 2. Results of Unconfined compressive strength (UCS), Point load strength, and Fracture distribution in rocks after FT cycles

Rock Types	Number of cycles		
	0 Cycle	50 Cycles	100 Cycles
UCS (MPa)			
DL	110	105	99
RY	81	75	70
GN	121	117	112
S.ST	42	36	30
L.ST	49	44	38
QZ	92	87	81
HGN	68	62	56
AM	129	126	120
GG	134	132	128
Point load (MPa)			
DL	49	46	44
RY	39	36	32
GN	51	48	46
S.ST	21	18	14
L.ST	28	25	21
QZ	43	40	37
HGN	34	31	27
AM	56	54	52
GG	64	62	60
UPV (m/s)			
DL	5107	4900	4687
RY	4511	4281	4081
GN	5298	5108	4911
S.ST	3275	3029	2765
L.ST	3567	3329	3090
QZ	4941	4718	4511
HGN	4186	3950	3716
AM	5488	5311	5128
GG	5791	5640	5461
Fracture density (%)			
DL	----------	0.49	1.12
RY	----------	0.59	1.22
GN	----------	0.48	1.08
S.ST	----------	1.12	1.47
L.ST	----------	1.06	1.44
QZ	----------	0.57	1.14
HGN	----------	0.76	1.31
AM	----------	0.46	1.03
GG	----------	0.43	1.02

5.5 Porosity, Water absorption, and Specific gravity

The porosity test results at the studied temperatures are shown in (Fig. 9C). Following freeze-thaw cycles, the samples' overall porosity increased, presumably as a result of an increase in fracture intensity.

After 100 cycles, the porosity values of dolerite, rhyolite, gabbronorite, quartzite, granitic gneiss, amphibolite, and granulite increased by 6.62%, 8.07%, 4.27%, 7.21%, 8.69%, 3.04%, and 2.79%, respectively. Furthermore, after the same number of cycles, the porosity of sandstone increased by 13% and that of limestone by 10.35%. The water absorption measurements also show a comparable rise (Fig. 9D). After 100 cycles, the percentage increase in water absorption for the rocks is as follows: granitic gneiss by 9.77%, rhyolite by 8.15%, quartzite by 6.93%, dolerite by 6.2%, gabbronorite by 5.75%, amphibolite by 4.65%, and granulite by 3.1%. In addition, after 100 cycles, the water absorption of sandstone rose to 15.34% and that of limestone to 12.1%.

The investigation's findings show that freeze-thaw affects specific gravity, as shown in (Fig. 9E). As the number of cycles increases, a visible decline becomes apparent. After 100 cycles, the percentage decreases in the specific gravity of the rock samples under study are as follows: granitic gneiss by 1.73%, rhyolite by 1.29%, dolerite by 1%, quartzite by 1.21%, gabbronorite by 0.99%, amphibolite by 0.69%, and granulite by 0.4%. After the same number of cycles, the specific gravity of sandstone declined by up to 1.89% and that of limestone by up to 1.63%.

5.6 UPV

According to experimental results, the UPV values of rock samples decrease as the number of freeze-thaw cycles increases (Fig. 9F). First, there was a small difference in UPV; however, as the number of cycles increased, UPV significantly decreased. After 100 cycles, the UPV values decreased as follows: granitic gneiss by 11.22%, rhyolite by 9.53%, dolerite by 8.22%, quartzite by 8.70%, gabbronorite by 7.30%, amphibolite by 6.56%, and granulite by 5.69%. After the same number of cycles, there is a reduction in the UPV of sandstone by 15.56% and limestone by 13.37%. These results emphasize that freeze-thaw affects porosity, specific gravity, UPV, and water absorption. It also highlights how crucial it is to take temperature changes into account when evaluating the mechanical qualities and integrity of rocks.

Table 3. Results of Porosity, Water absorption, and Specific gravity of studied rocks before and after freeze-thaw cycles

Rock Types	Number of cycles		
	0 Cycle	50 Cycles	100 Cycles
Porosity (%)			
DL	0.64	0.65	0.68
RY	1.15	1.20	1.25
GN	0.49	0.50	0.56
S.ST	2.54	2.77	2.92
L.ST	1.98	2.11	2.21
QZ	0.95	0.98	1.03
HGN	1.71	1.79	1.88
AM	0.35	0.36	0.36
GG	0.31	0.32	0.32
Water absorption (%)			
DL	0.24	0.25	0.26
RY	0.45	0.48	0.49
GN	0.21	0.22	0.23
S.ST	1.58	1.75	1.87
L.ST	1.35	1.48	1.54
QZ	0.34	0.35	0.36
HGN	0.55	0.60	0.61
AM	0.16	0.17	0.17
GG	0.13	0.13	0.13
Specific gravity			
DL	2.98	2.97	2.95
RY	2.78	2.77	2.75
GN	3.12	3.12	3.09
S.ST	2.65	2.63	2.56
L.ST	2.71	2.69	2.66
QZ	2.88	2.87	2.85
HGN	2.72	2.70	2.68
AM	3.16	3.16	3.14
GG	3.22	3.22	3.21

6 Discussion

The impacts of freeze-thaw cycles on the physico-mechanical properties of rocks vary depending on the composition of the minerals, textural relations, individual mineral behavior, and the fracture and deformational nature of the rocks. For every type of rock, UCS, UPV, and porosity were measured after 100 freeze-thaw cycles. The values are given in Tables 2 and 3 and (Figs. 9 and 10).

Every rock's porosity increased along with a drop in UCS and UPV due to cycle progression, as seen in Tables 2 and 3. These changes vary from rock to rock. The rock deterioration degree is indicated by the increase-decrease ratio, which ranges from 0 to 1. Rocks that had degraded at the end of the F–T cycles are given a rating value of 1. On the other hand, a grade of 0 denotes the strongest type of rock. These data show the deterioration grade in ascending order, and vice versa.

Using the following formula, the increased porosity ratio at the conclusion of the 50 and 100 F-T cycles was determined (Khanlari et al., 2015).

$$Rp = P_{(nc)}/P_{(us)}-1$$

Where $P_{(nc)}$ is the total porosity at the end of specific number of freeze-thaw cycles and $P_{(us)}$ is the total porosity of untreated rock types. The Rp values are given in Table 4; trends in Rp values are shown in (Fig. 10A).

Table 4. Rp, Rvp and SDR values of samples after 50 and 100 F-T cycles

50 CYCLES			
Rock Types	Rp	Rvp	SDR
DL	0.030	0.041	0.045
RY	0.043	0.051	0.074
GN	0.022	0.036	0.033
S.ST	0.091	0.075	0.143
L.ST	0.066	0.067	0.102
QZ	0.033	0.045	0.054
HGN	0.046	0.056	0.088
AM	0.017	0.032	0.023
GG	0.016	0.026	0.015
100 CYCLES			
DL	0.071	0.082	0.1
RY	0.088	0.095	0.136
GN	0.045	0.073	0.075
S.ST	0.150	0.156	0.286
L.ST	0.116	0.134	0.224
QZ	0.078	0.087	0.120
HGN	0.095	0.112	0.177
AM	0.031	0.066	0.070
GG	0.029	0.057	0.045

As shown in Tables 3 and 4, sample granulite exhibits the lowest increase in porosity at the end of the 100 F-T cycles, with Rp100 of 0.029 (2.9%), whereas sandstone displays the most increase with Rp100 of 0.150 (15%). The number of pores in the samples is thought to be related to these changes. During the freezing process, the water in the pore's contracts due to which its volume increases, causing the pores to expand. As seen in Figures 6, 7, and 8, new cracks and pores develop in the rock, depending on how much of these processes have occurred. The trends of the samples' porosity change are displayed in Figure 10A.

In the F-T cycle, groundwater or surface water enters the rock through capillary action, increases in volume, and exerts pressure inside the pores and discontinuities where it freezes. This cycle keeps happening, creating adverse deterioration of the rock (Su et al., 2024). When water freezes and thaws, weakening, breakdowns, and expansion lead to the production of cracks and fractures in rocks with a high-water absorption capacity, making the decline in the strength of the rock more noticeable.

Using a similar approach, the decrease in ratios of UPV at the end of the 50 and 100 cycles was calculated by using the following equation (Khanlari et al., 2015):

$$R_{VP} = 1\text{-}Vp_{(nc)}/Vp_{(us)}$$

Where $Vp_{(nc)}$ is the P wave velocity of rock samples at the end of 100 freeze-thaw cycles and $Vp_{(us)}$ is the P wave velocity of untreated rocks.

Tables 2 and 4 along with the Figures. 9F and 10B demonstrate how advancing the F-T cycles resulted in declining trends for UPV. The findings show that the freeze-thaw cycles caused the most damage to the sandstone samples amongst all rock types, with a decreased ratio of Rvp100 of 0.156 which indicates a 15.6 % reduction in UPV. On the contrary, the granulite sample had the least decrease of Rvp100 which is 0.057 which means a 5.7 % reduction in UPV.

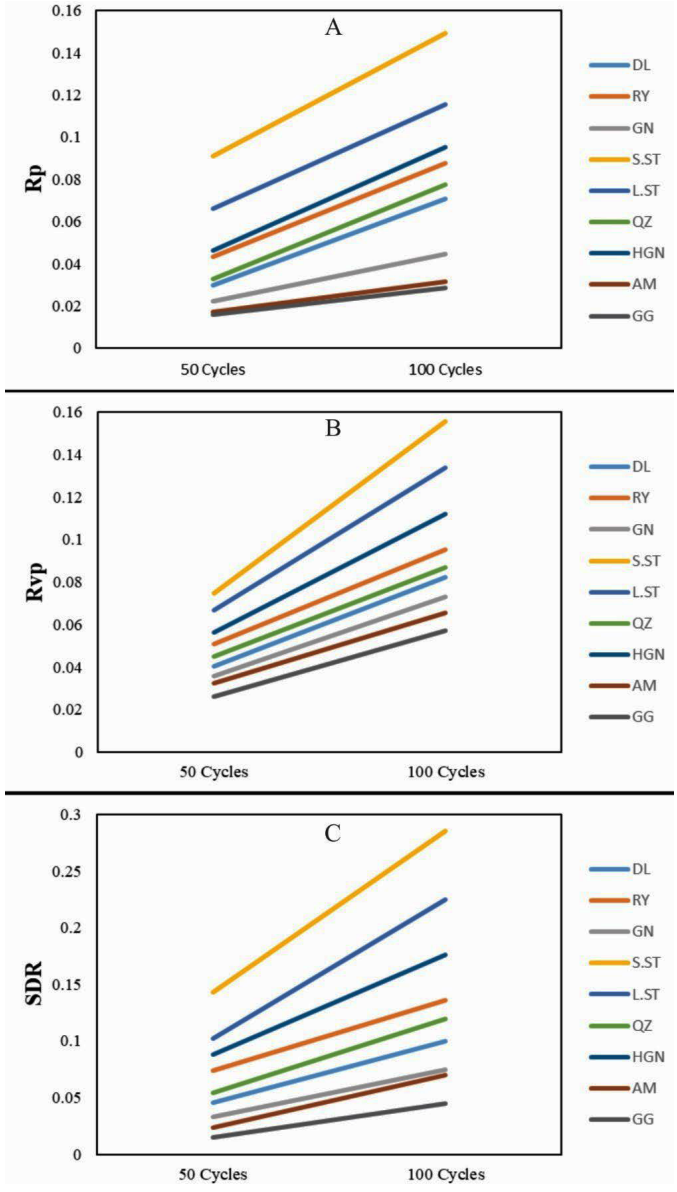

Figure 10. Trends in Rp (A), Rvp (B), and SDR(C) of the studied samples.

Strength Deterioration Ratio (SDR) at the end of F–T cycles was calculated using the following equation (Khanlari et al., 2015):

$$SDR = 1\text{-}UCS\ (nc)/UCS\ (us)$$

Where $UCS_{(nc)}$ is the uniaxial compressive strength of rock samples at the end of number of freeze-thaw cycles and $UCS_{(us)}$ is the strength of untreated samples. The strength deterioration values of rocks are given in Table 4 and the

trends of decrease ratios are given in (Fig. 10C). Sandstone samples represent the most sensitive rocks of all the samples with the highest strength deterioration rate of 0.286. However, the granulite sample had the least damage with an SDR value of 0.045.

Mitigation Strategies for Freeze-Thaw Damage

7 Mitigation Strategies for Freeze-Thaw Damage

Freeze-thaw cycles can significantly impact the durability of sandstone and limestone constructions, leading to microcracking, increased porosity, and structural weakening over time. To mitigate these effects, several strategies can be implemented, focusing on reducing water infiltration, enhancing material strength, and improving environmental management.

7.1 Surface Treatments and Sealants

Applying hydrophobic coatings or sealants can effectively reduce water absorption in porous rocks like sandstone and limestone. These treatments create a protective layer that prevents moisture penetration while allowing the material to breathe, reducing internal stress caused by freeze-thaw cycles. However, the selection of sealants should consider permeability to avoid trapping moisture within the stone, which could exacerbate damage.

7.2 Improved Drainage Systems

Proper drainage around structures is crucial to minimizing water exposure. Installing adequate gutters, sloping surfaces, and subsurface drainage systems can help divert water away from foundations and rock surfaces, limiting prolonged saturation and reducing the potential for freeze-thaw deterioration.

7.3 Material Selection and Reinforcement

Using more durable rock variants or combining sandstone and limestone with reinforcing materials can enhance structural resilience. In construction, selecting denser, lower-porosity stone reduces vulnerability to freeze-thaw damage. Additionally, incorporating protective barriers, such as waterproof membranes or composite materials, can improve longevity.

7.4 Environmental and Maintenance Strategies

Regular maintenance, such as cleaning debris, inspecting cracks, and applying protective coatings when necessary, ensures long-term preservation. In colder climates, minimizing direct exposure to de-icing salts, which can accelerate chemical weathering and porosity increase, is also essential. Additionally, designing structures with overhangs or protective facades can shield rock surfaces from excessive moisture accumulation.

By implementing these mitigation strategies, sandstone and limestone constructions can better withstand freeze-thaw cycles, prolonging their lifespan and structural integrity in harsh climatic conditions.

8. Conclusions

This study extensively examined how freeze-thaw cycles impact the physico-mechanical characteristics of rocks, including porosity, specific gravity, water absorption, and ultrasonic pulse wave velocity (UPV). Various volcanic, sedimentary, and metamorphic rock samples underwent multiple freeze-thaw cycles, with their properties assessed at different stages. The results revealed significant variations in mechanical properties, emphasizing the importance of considering freeze-thaw effects in geological and engineering contexts, particularly in regions with fluctuating temperatures around the freezing point of water, such as northern Pakistan and similar climates. Understanding rock deterioration processes due to freeze-thaw weathering is crucial. This research is relevant for engineering applications in cold regions, aiding in construction and maintenance, especially where snowfall is frequent. From this study, the following conclusions are drawn:

- P-wave velocity, point load strength, specific gravity, and uniaxial compressive strength were shown to decrease with an increase in the number of freeze-thaw cycles, although porosity and water absorption values showed a positive trend.
- Fracture density considerably increased with freeze-thaw cycling resulting in the disintegration of rocks.
- Sandstone exhibited pronounced porosity increase and reduced P-wave velocity, correlating with higher Strength Deterioration Ratios (SDR), highlighting its vulnerability to freeze-thaw cycles. Conversely, granulite, with lower porosity and minimal P-wave velocity reduction, shows comparatively lower SDR values, emphasizing the crucial role of porosity and P-wave velocity in assessing rock stability.

Acknowledgments

The authors would like to acknowledge the National Centre of Excellence in Geology at the University of Peshawar (Pakistan) for providing laboratory facilities and field logistics.

Funding

This research received no external funding

Data availability

All data are included in the manuscript.

Declaration

Conflict of interest

The authors declare that they have no known competing financial interests or personal relationships that could have appeared to influence the work reported in this paper.

References

Ali, A., Ahmad, S., Ahmad, S., Khan, M.A, Khan, M.I. and Rehman, G., 2021. Tectonic Framework of Northern Pakistan from Himalaya to Karakoram. Structural Geology and Tectonics Field Guidebook—Volume 1, pp.367-412.

Arif, M., Jan, M.Q., 2006. Petrotectonic significance of the chemistry of chromite in the ultramafic–mafic complexes of Pakistan. J. Asian. Earth. Sci. 27, 628-646.

Asif, A.R., Islam, I., Ahmed, W., Sajid, M., Qadir, A., Ditta, A., 2022. Exploring the potential of Eocene carbonates through petrographic, geochemical, and geotechnical analyses for their utilization as aggregates for engineering structures. Arab. J. Geosci. 15, 1–19.

Asif, A.R., Sajid, M., Ahmed, W., Nawaz, A., 2024. Weathering effects on granitic rocks in North Pakistan: petrographic insights, strength classifications, and construction suitability. Environ. Earth. Sci. 83, 351.

Bell, F., Jermy, C., 2000. The geotechnical character of some South African dolerites, especially their strength and durability. QJEGH. 33, 59-76.

Bellanger, M., Homand, F., Remy, J., 1993. Water behavior in limestones as a function of pores structure: application to frost resistance of some Lorraine limestones. Eng Geol. 36, 99-108.

Binal, A., Kasapoglu, K., Sensogut, C., Ozkan, I., 2002. In Effects of freezing and thawing process on physical and mechanical properties of Selime ignimbrite outcrops in Aksaray–Ihlara valley, VI Regional Rock Mechanics Symposium. Turkish National Society for Rock Mechanics, Seljuk University, Konya. p 196.

Burg, J.P., 2018. Geology of the onshore Makran accretionary wedge: Synthesis and tectonic interpretation. Earth-Sci. Rev. 185, 1210-1231.

Cawood, P.A., Johnson, M.R., Nemchin, A.A., 2007. Early Palaeozoic orogenesis along the Indian margin of Gondwana: Tectonic response to Gondwana assembly. EPSL. 255, 70-84.

Chen, L., Li, K., Song, G., Zhang, D., Liu, C., 2021. Effect of freeze–thaw cycle on physical and mechanical properties and damage characteristics of sandstone. Sci. Rep. 11(1), 12315.

Chen, T., Ji, S., Foulger, G. R., & Gong, B., 2023. Fracture spacings of fiber inclusions in a ductile geological matrix and development of microboudins: 3D numerical modeling. J. Struct. Geol. 174, 104920.

Chen, T., Yeung, M., Mori, N., 2004. Effect of water saturation on deterioration of welded tuff due to freeze-thaw action. Cold Reg. Sci. Technol. 38, 127-136.

Chen, Y., Lin, H., Liang, L., 2023. Freeze-thaw failure characteristics and strength loss of non-penetrating fractured rock mass with different fracture densities. THEOR APPL FRACT MEC. 124, 103792.

Citak, H., Coramik, M., Gunes, H., Bicakci, S., & Ege, Y., 2023. Comprehensive Review of Studies on Metamorphic Rocks. IJG, 14(10), 999-1035.

Claridge, G.G.C., & Campbell, I.B., 2005. Weathering processes in arid cryosols. In Cryosols: Permafrost-Affected Soils (pp. 447-458). Berlin, Heidelberg: Springer Berlin Heidelberg.

Coward, M., Butler, R., Khan, M.A., Knipe, R., 1987. The tectonic history of Kohistan and its implications for Himalayan structure. J. Geol. Soc. 144, 377-391.

Deprez, M., De Kock, T., De Schutter, G., & Cnudde, V., 2020. A review on freeze-thaw action and weathering of rocks. Earth-Sci. Rev. 203, 103143.

Dhuime, B., Bosch, D., Bodinier, J.L., Garrido, C., Bruguier, O., Hussain, S.S., Dawood, H., 2007. Multistage evolution of the Jijal ultramafic–mafic complex (Kohistan, N Pakistan): implications for building the roots of island arcs. EPSL. 261, 179-200.

DiPietro, J.A., Isachsen, C.E., 2001. U-Pb zircon ages from the Indian plate in northwest Pakistan and their significance to Himalayan and pre-Himalayan geologic history. Tectonics. 20, 510-525.

Fener, M., İnce, İ., 2015. Effects of the freeze–thaw (F–T) cycle on the andesitic rocks (Sille-Konya/Turkey) used in construction building. J. Afr. Earth. Sci. 109, 96-106.

Fujun, N., Guodong, C., Huimin, X., Lifeng, M., 2006. Field experiment study on effects of duct-ventilated railway embankment on protecting the underlying permafrost. Cold. Reg. Sci. Technol. 45, 178-192.

Grossi, C.M., Brimblecombe, P., Harris, I., 2007. Predicting long-term freeze–thaw risks on Europe built heritage and archaeological sites in a changing climate. Sci. Total. Environ. 377, 273-281.

Halsey, D., Mitchell, D., Dews, S., 1998. Influence of climatically induced cycles in physical weathering. QJEGH. 31, 359-367.

Hou, J., Li, J., Yang, D., Wang, B., 2025. Meso-mechanical Damage and Energy Dissipation Mechanism in Backfill: Effects of Seepage and Crack Defects. Geotech. Geol. Eng. 43(1), 1-18.

Islands, W., McMurdo, H., Valleys, D., South, S. S., Odbert, I., & Ridge, R., 2002. 42 RD Seppelt. Geoecology of Antarctic Ice-Free Coastal Landscapes: With 59 Tables, 154, 42.

Jadoon, U.K., Ding, L., Baral, U., Qasim, M., 2020. Early Cretaceous to Eocene magmatic records in Ladakh arc: Constraints from U–Pb ages of Deosai volcanics, northern Pakistan. Geol. J. 55(7), 5384-5397.

Jain, A., Mukherjee, P., Singhal, S., 2020. Terrane characterization in the Himalaya since Paleoproterozoic. Episodes J. Int. Geosci. 43(1), 346-357.

Jan, M.Q., 1988. Geochemistry of amphibolites from the southern part of the Kohistan arc, N. Pakistan. Mineral. Mag. 52, 147-159.

Jan, M.Q., Howie, R., 1981. The mineralogy and geochemistry of the metamorphosed basic and ultrabasic rocks of the Jijal complex, Kohistan, NW Pakistan. J. Petrol. 22, 85-126.

Kaczmarek, H., 2021. Thermal conditions of freeze-thaw processes on the cliff face in winter 2019-2020 on the Jeziorsko Reservoir, central Poland. Geog Tour, 2(9), 59-66.

Kaczmarek, H., Bartczak, A., Tyszkowski, S., Badocha, M., Krzemiński, M., 2021. The impact of freeze-thaw processes on a cliff recession rate in the face of temperate zone climate change. Catena. 202, 105259.

Khan, M.A., Jan, M.Q., Weaver, B., 1993. Evolution of the lower arc crust in Kohistan, N. Pakistan: temporal arc magmatism through early, mature and intra-arc rift stages. Geol. Soc. Spec. Publ. 74, 123-138.

Khanlari, G., Sahamieh, R.Z., Abdilor, Y., 2015. The effect of freeze–thaw cycles on physical and mechanical properties of Upper Red Formation sandstones, central part of Iran. Arab. J. Geosci. 8, 5991-6001.

King, J., Harris, N., Argles, T., Parrish, R., Zhang, H., 2011. Contribution of crustal anatexis to the tectonic evolution of Indian crust beneath southern Tibet. Geol. Soc. Am. Bull. 123, 218-239.

Kolhe, A.R., Thorat, V.S., Gorde, P.J., Chandgude, M.S.E., 2024. Text book of building construction and construction materials. Academic Guru Publishing House.

Le Fort, P., 1986. Metamorphism and magmatism during the Himalayan collision. Geol. Soc. Spec. Publ. 19,159-172.

Liu, C., Lv, Y., Yu, X., & Wu, X., 2020. Effects of freeze-thaw cycles on the unconfined compressive strength of straw fiber-reinforced soil. Geotext. Geomembr, 48(4), 581-590.

Liu, Y., Cai, Y., Huang, S., Guo, Y., Liu, G., 2020. Effect of water saturation on uniaxial compressive strength and damage degree of clay-bearing sandstone under freeze-thaw. Bull. Eng. Geol. Environ. 79, 2021-2036.

Lutfi, W., Sheikh, L., Zhao, Z., Song, S., Zafar, T., Rahim, Y., Liu, D., Zhu, D.C., Wang, Z., Ahmad, L., 2023. Making the Juvenile lower continental crust by melting of contaminated oceanic mantle wedge: Evidence from the Chilas Complex in the Kohistan Island Arc, North Pakistan. Lithos. 436, 106952.

Maľa, M., Greif, V., & Ondrášik, M. (2024). Deterioration of volcanic tuffs from rock dwellings in Brhlovce (Slovakia) induced by freeze-thaw cycling studied by non-destructive tests and μCT visualization. BOEG, 83(5), 166.

Maľa, M., Greif, V., Ondrášik, M., 2024. Deterioration of volcanic tuffs from rock dwellings in Brhlovce (Slovakia) induced by freeze-thaw cycling studied by non-destructive tests and μCT visualization. Bull. Eng. Geol. Environ. 83(5), 1-15.

Mutlutürk, M., Altindag, R., Türk, G., 2004. A decay function model for the integrity loss of rock when subjected to recurrent cycles of freezing–thawing and heating–cooling. Int. J. Rock. Mech. Min. Sci. 41, 237-244.

Niu, C., Zhu, Z., Zhou, L., Li, X., Ying, P., Dong, Y., & Deng, S., 2021. Study on the microscopic damage evolution and dynamic fracture properties of sandstone under freeze-thaw cycles. Cold Reg. Sci. Technol. 191, 103328.

Noble, S., Searle, M., Walker, C., 2001. Age and tectonic significance of Permian granites in western Zanskar, High Himalaya. J. Geol. 109, 127-135.

Park, N.K., 2004. A guide to using event study methods in multi-country settings. STRATEGIC. MANAGE. J. 25, 655-668.

Pei, Q.Y., Zou, W.L., Han, Z., Wang, X.Q. and Xia, X.L., 2024. Compression behaviors of a freeze–thaw impacted clay under saturated and unsaturated conditions. Acta. Geot. 1-18.

Proskin, S., Sego, D., Alostaz, M., 2010. Freeze–thaw and consolidation tests on Suncor mature fine tailings (MFT). Cold. Reg. Sci. Technol. 63, 110-120.

Qureshi, J.A., Ali, K., Murad, S., Ali, A., Khan, G., Ali, M. and Alam, M., 2020. The preliminary investigation and mineral characterization of the Gold and Copper at Gindai Yasin, Ghizer, Pakistan. JHES. 53(2).

Rehman, S.U. and Arif, M., 2020. Gabbronorite from Jijal Complex, Kamila Amphibolite Belt and Chilas Complex, Northern Pakistan: Implications for Arc Genesis. IJEEG. 11(3), 70-78.

Ringuette, L., Martignole, J., 1999. Windley, B.F.: Magmatic crystallization, isobaric cooling, and decompression of the garnet-bearing assemblages of the Jijal sequence (Kohistan terrane, western Himalayas). Geology. 27, 139-142.

Sajid, M., Andersen, J., Rocholl, A., & Wiedenbeck, M., 2018. U-Pb geochronology and petrogenesis of peraluminous granitoids from northern Indian plate in NW Pakistan: Andean type orogenic signatures from the early Paleozoic along the northern Gondwana. Lithos, 318, 340-356.

Schwamborn, G., Schirrmeister, L., Frütsch, F., & Diekmann, B., 2012. Quartz weathering in freeze–thaw cycles: Experiment and application to the El'gygytgyn Crater Lake record for tracing Siberian permafrost history. Geografiska Annaler: Series A, Physical Geography, 94(4), 481-499.

Searle, M., Khan, M.A., Fraser, J., Gough, S., Jan, M.Q., 1999. The tectonic evolution of the Kohistan-Karakoram collision belt along the Karakoram Highway transect, north Pakistan. Tectonics. 18, 929-949.

Searle, M., Treloar, P., 2010. Was Late Cretaceous–Paleocene obduction of ophiolite complexes the primary cause of crustal thickening and regional metamorphism in the Pakistan Himalaya? Geol. Soc. Spec. Publ. 338, 345-359.

Searle, M.P., 2011. Geological evolution of the Karakoram Ranges. Ital. J. Geosci. 130, 147-159.

Sen, A., Sen, K., Chatterjee, A., Choudhary, S. and Dey, A., 2022. Understanding pre-and syn-orogenic tectonic evolution in western Himalaya through age and petrogenesis of Palaeozoic and Cenozoic granites from upper structural levels of Bhagirathi Valley, NW India. Geol. Mag. 159(1), 97-123.

Simonsen, E., Isacsson, U., 1999. Thaw weakening of pavement structures in cold regions. Cold. Reg. Sci. Technol. 29, 135-151.

Soret, M., Larson, K.P., Cottle, J. and Ali, A., 2021. How Himalayan collision stems from subduction. Geol. 49(8), 894-898.

Su, X.L., Zhang, C.P., Zou, Z.X., Wang, Y., Lai, J. and Liu, T., 2024. Influence of water rock interaction on stability of tunnel engineering. Pol. J. Environ. Stud.

Suo, Y., Li, S., Cao, X., Dong, H., Li, X. and Wang, X., 2022. Two-stage eastward diachronous model of India-Eurasia collision: Constraints from the intraplate tectonic records in Northeast Indian Ocean. Gond. Res. 102, 372-384.

Takarli, M., Prince, W., Siddique, R., 2008. Damage in granite under heating/cooling cycles and water freeze–thaw condition. Int. J. Rock. Mech. Min. Sci. 45, 1164-1175.

Talalay, P.G., 2023. Drilling Challenges and Drilling Methods in the Polar Regions. In Geotechnical and Exploration Drilling in the Polar Regions (pp. 43-80). Cham: Springer International Publishing.

Talalay, P.G., 2024. Underground Mining and Construction in Snow and Ice. Mining and Construction in Snow and Ice: From Test Pits to Long Tunnels, 219-252.

Talalay, P. G., Drilling Targets in the Polar Regions. In Geotechnical and Exploration Drilling in the Polar Regions, Springer: 2023; pp 1-42.

Talalay, P.G., 2022. Geotechnical and Exploration Drilling in the Polar Regions. Springer.

Treloar, P., Broughton, R., Williams, M., Coward, M., Windley, B., 1989. Deformation, metamorphism and imbrication of the Indian plate, south of the Main Mantle Thrust, north Pakistan. J. Metamorph. Geol. 7, 111-125.

Treloar, P.J., Petterson, M.G., Jan, M.Q., Sullivan, M., 1996. A re-evaluation of the stratigraphy and evolution of the Kohistan arc sequence, Pakistan Himalaya: implications for magmatic and tectonic arc-building processes. J. Geol. Soc. 153, 681-693.

Ullaha, H., Rehmana, S.U., Munawara, M.J. and Abbasa, S.A., 2022. Petrogenetic Importance of Chromite Chemistry in Ophiolites, Mafic-Ultramafic Complexes NW, Pakistan & Ranomena Ultramafic Complex NE, Madagascar: A review. J. Earth Sci. 3(2), 29-51.

Wang, Y., Xing, X., Cawood, P.A., Lai, S., Xia, X., Fan, W., Liu, H., Zhang, F., 2013. Petrogenesis of early Paleozoic peraluminous granite in the Sibumasu Block of SW Yunnan and diachronous accretionary orogenesis along the northern margin of Gondwana. Lithos. 182, 67-85.

Yamabe, T., Neaupane, K.M., 2001. Determination of some thermo-mechanical properties of Sirahama sandstone under subzero temperature condition. Int. J. Rock. Mech. Min. Sci. 38, 1029-1034.

Zeitler, P.K., 1985. Cooling history of the NW Himalaya, Pakistan. Tectonics. 4, 127-151.

Zhao, P., Wang, Y., Xu, Z., Chang, X., & Zhang, Y., 2024. Research progress of freeze–thaw rock using bibliometric analysis. Open Geosci. 16(1), 20220663.

Zhao, Y., Hu, K., Han, D., Lang, Y., Zhang, L., 2024. Multifactor-coupled study on freeze-thaw forces of rocks in cold regions. Front. Earth Sci. 12, 1404153.

Zhou, X.P., Li, C.Q., Zhou, L.S., 2020. The effect of microstructural evolution on the permeability of sandstone under freeze-thaw cycles. Cold Reg. Sci. Technol. 177, 103119.